



ADM Solution for Cu/CuO –Water Viscoplastic Nanofluid Transient Slip Flow from a Porous Stretching Sheet with Entropy Generation, Convective Wall Temperature and Radiative Effects

Thirupathi Thumma¹, S.R. Mishra², O. Anwar Bég³

¹ Department of Mathematics, B V Raju Institute of Technology, Narsapur, Medak, 502313, Telangana State, India. Email: thirupathireddy.t@bvrit.ac.in

² Department of Mathematics, Siksha 'O' Anusandhan Deemed to be University, Bhubaneswar, 751030, Odisha, India. Email: satyaranjan_mshr@yahoo.co.in

³ Fluid Mechanics, Propulsion and Nanosystems, Aeronautical and Mechanical Engineering, Newton Bldg., University of Salford, Manchester, M54WT, UK. Email: O.A.Beg@salford.ac.uk

Received April 03 2020; Revised June 12 2020; Accepted for publication June 15 2020.

Corresponding author: T. Thumma (thirupathireddy.t@bvrit.ac.in)

© 2021 Published by Shahid Chamran University of Ahvaz

Abstract. A mathematical model is presented for entropy generation in transient hydromagnetic flow of an electroconductive magnetic Casson (non-Newtonian) nanofluid over a porous stretching sheet in a porous medium. The model employed is Cattaneo-Christov heat flux to simulate non-Fourier (thermal relaxation) effects. A Rosseland flux model is implemented to model radiative heat transfer. The Darcy model is employed for the porous media bulk drag effect. Momentum slip is also included to simulate non-adherence of the nanofluid at the wall. The transformed, dimensionless governing equations and boundary conditions (featuring velocity slip and convective temperature) characterizing the flow are solved with the Adomian Decomposition Method (ADM). Bejan's entropy minimization generation method is employed. Cu-water and CuO-water nanofluids are considered. Extensive visualization of velocity, temperature, and entropy generation number profiles is presented for variation in pertinent parameters. The calculation of skin friction and local Nusselt number are also studied. The ADM computations are validated with simpler models from the literature. The solutions show that with elevation in the volume fraction of nanoparticle and Brinkman number, the entropy generation magnitudes are increased. An increase in Darcy number also upsurges the friction factor and heat transfer at the wall. Increasing volume fraction, unsteadiness, thermal radiation, velocity slip, Casson parameters, Darcy, and Biot numbers are all observed to boost temperatures. However, temperatures are reduced with increasing non-Fourier (thermal relaxation) parameter. The simulations are relevant to the high temperature manufacturing fluid dynamics of magnetic nano liquids, smart coating systems.

Keywords: Cattaneo-Christov (Non-Fourier) Heat Flux Model; Casson Nanofluid, Adomian Decomposition Method; Convective and Slip Conditions; Porous Media; Magnetohydrodynamic Materials Processing.

1. Introduction

This A new subgroup of nanofluids in energy sciences called magnetic nanofluids has transpired which evince both thermal and magnetic enhancement properties. In general, the exploitation of nano-sized particles in a traditional fluid, namely ethylene glycol, oil, and water to achieve thermal enhancement was proposed by Choi [1]. Subsequently, numerous mathematical models were presented to explain the Thermophysics of nanofluids and such approaches have featured many sophisticated phenomena including particle Brownian motion (ballistic collisions) and thermophoresis which provide a reasonable platform for clarifying the observed increase in thermal conductance of nanofluids (Buongiorno [2]). Conventional heat transfer fluids exhibit inferior cooling rates compared with nanofluids. Hence nanofluids offer substantially higher thermal efficiency than the base fluids. Magnetic nanofluids have the additional advantage that they can be manipulated via external magnetic fields and in this sense function as "smart" fluids. Some diverse applications of magneto nanofluid technology are magnetic drug targeting in hemodynamics, biomedical cancer therapy, smart lubrication, intelligent coating systems, etc. Numerical studies of such fluids have stimulated some interest in industrial sciences in the latest ages. In the synthesis of magnetic nanofluids for coating systems, fluid dynamics play a key role. Important applications also arise in hybrid solar collectors (direct absorber systems). Several authors have examined this topic in recent years. Khan et al. [3] reported on entropy generation minimization in MHD flow of nanofluid over a stretching surface. Zohra et al. [4] considered Falkner-Skan boundary layer flows of magnetic nanofluids (also doped with Bio convective micro-organisms) with Maple quadrature. Khan et al. [5] considered the tangent hyperbolic nanofluid model in nonlinear mixed convection to study the optimization of the entropy generation. Prakash et al. [6] studied magnetic nanofluid bio-inspired solar collectors with perturbation methods. Li et al. [7] observed in their experimentation that the thermal conductivity of paraffin nanofluid is enhanced with a mass fraction of SiO₂ nanoparticles. Kumar et al. [8] simulated



the time-dependent polar magnetic nanofluid Sakiadis coating flow with Joule electrical dissipation. Ray et al. [9] employed homotopy and generalized differential quadrature methods to compute the heat, momentum, and mass transfer characteristics in transient non-Newtonian magnetic nanofluid flow from an extending sheet. Ngiangia and Akaezue [10] used the Tiwari-Das model to study mixed convection radiative Magnetohydrodynamic flow of copper nanofluid (with different nano-particle shapes) with chemical reaction effects. Recently, on thermal conductivity experimental investigations, Li et al. [11] reported Phase Change Materials (PCM) in the presence of porosity and nanoparticles. Ma et al. [12] adopted the FVM (Finite Volume Method) for investigating the solidification inside the wavy duct by suspending CuO nanoparticles into the paraffin pure PCM. On MHD Carreau radiative nanofluid, Bhatti et al. [13] investigated the entropy analysis over a shrinking surface.

Historically Fourier [14] established that heat interchange happens due to temperature deviation among different bodies as embodied in Fourier thermal conduction law. Cattaneo [15] extended Fourier's heat conduction law by incorporating thermal relaxation time. Christov [16] further extended this by considering finite-speed heat conduction (finite thermal waves). In recent years there has been a resurgence in interest in the so-called Cattaneo-Christov heat flux model (non-Fourier) since it provides more elegant thermo physical details than the Fourier model. In the context of non-Newtonian (e.g. Casson viscoplastic) nanofluids, some representative studies are available in [17-19]. In modern thermal materials processing and energy systems design, entropy generation minimization (EGM) has also become a significant area of research. Asif et al. [20] used a finite difference method to analyze entropy and heat transfer effects on Casson nanofluid dynamics. Ibrahim and Makinde [21] have presented numerical solutions for Magnetohydrodynamic (MHD) stream of Casson nanofluid for various slip and convective conditions. A similar study was undertaken with the Keller Box Method (KBM) considering Joule heating by Kamran et al. [22]. Nadeem et al. [23] developed results for 3-dimensional Casson Sakiadis flow embedded within a porous medium. Hussain et al. [24] conducted a study of Casson magnetic nanofluid flow from an expanding surface with Ohmic magnetic dissipation and wall slip effects. Recently, a similar numerical study has performed for Casson nanofluids by Sulochana et al. [25]. Abolbashari et al. [26] presented homotopy solutions for entropy generation in stretching sheet Casson nanofluid transport. Wasim and Asim [27] presented Keller box finite difference numerical solutions for entropy generation in Casson nanofluid flow due to an elongating sheet. Qing et al. [28] explored entropy generation on MHD flow of Casson nanofluid over a permeable surface. Li et al. [29] studied Nano-clay content effects on the density of PVC matrix foam, they reported that the thermal conductivity is affected. Further studies on Casson nanofluid flow from a stretching sheet are documented in [30-33]. These analyses are all relevant to nanomaterial extrusion and fabrication processes.

Invariably manufacturing nanofluid dynamics generates highly nonlinear and coupled partial differential equation boundary value problems. Such models prohibit the extraction of closed-form solutions. Different semi-numerical/analytical and numerical techniques have therefore been employed in studying such flows. A particularly versatile and accurate semi-analytical/numerical methods are ADM (Adomian Decomposition Method). Adomian [34-35] pioneered this technique which circumvents the need for discretization associated with grid-based numerical methods and permits the derivation of power-series based solutions for nonlinear equations. This method yields analytical solutions that can be evaluated with symbolic software e.g. MAPLE, MATHEMATICA, and MATLAB, etc. [36]. ADM has therefore been implemented extensively in multi-physical fluid mechanics (and other areas). Pertinent studies in this regard include Khan et al. [37] (Casson fluid between parallel plates), Srinivas et al. [38] (Micropolar flow through the vertical channel), Ebaid et al. [39] (for nanofluid flow), Manzoor et al. [40] (for magnetic bio rheological ciliated channel flow) and Opanuga et al. [41-42] (for couple stress fluids).

In the present article, motivated by nanomaterial manufacturing transport phenomena applications, a detailed analysis of entropy generating in unsteady Magnetohydrodynamic radiative Casson nanofluid flow from an elongating surface with dissipation effects in a porous medium is presented. A non-Fourier (Cattaneo-Christov) heat flux model is utilized which generalizes the classical Fourier law to incorporate thermal relaxation time effects. The leading partial differential conservation balances are rendered into ordinary differential form with suitable likeness transformations. The emergent nonlinear ordinary differential boundary value problem is solved with the Adomian decomposition method (ADM). Confirmation of results is encompassed for the distinct case of purely fluid media (i.e. infinite porousness of the leaky medium) with Asif et al. [20]. The influence of magnetic field parameter, unsteadiness parameter, and Casson parameter, the volume fraction of nanofluid, permeability parameter, suction/injection parameter, radiative parameter, Biot number, relaxation time parameter, velocity slip parameter, and Prandtl number on velocity and temperature distributions are visualized realistically. Skin friction and local Nusselt number values are also tabulated. An extensive interpretation is included. The study provides a deeper insight into the heat transfer phenomena in magnetic nanomaterial processing (manufacturing) systems.

2. Mathematical Model

The Study object is the transient, two-dimensional, laminar, incompressible, MHD dissipative boundary layer flow of an electrically conducting non-Newtonian Casson nanofluid from a porous elongating sheet embedded in anisotropic, Darcian porous medium under uni-directional radiative flux and a transverse magnetic field. A non-uniform stretching sheet velocity $U_w(x) = cx / (1 - \lambda t)$ along the direction of the x -axis is considered, where c is constant and $\lambda \geq 0$. The physical model is exemplified in Fig. 1. In the direction of normal to the sheet, a variable magnetic field $B = B_0 / \sqrt{1 - \lambda t}$ is applied, here B_0 is the strength of the magnetic field. The magnetic field is sufficiently weak to negate magnetic induction effects (low magnetic Reynolds number). The elongating porous sheet represents an electroconductive (magnetic) nano-polymer and is extruded by the stretching force along the x -axis from the fixed origin. The temperature at the elongating surface fluctuates with time and space while it is constant as $y \rightarrow \infty$, and is expressed as $T_w = T_\infty + ((cx) / (1 - \lambda t))$ where T_∞ is the temperature at the free-stream condition. The nanofluid is treated as a single-phase in thermal equilibrium and gravity effects are ignored. Furthermore, the following [4] no-slip arises between the base fluid molecules and nanoparticles. u_w, v_w & T_w They are in effect only for $t < (1 / \lambda)$ but not when $\lambda = 0$. The stress-strain relations for a Casson fluid take the form (See [9, 28]):

$$\tau_{ij} = \begin{cases} 2(\mu_B + (p_y / \sqrt{2\pi}))e_{ij}, & \pi > \pi_c \\ 2(\mu_B + (p_y / \sqrt{2\pi}))e_{ij}, & \pi < \pi_c \end{cases} \tag{1}$$

Using Eqn. (1), invoking the boundary layer approximations (Asif et al. [20]) and incorporating contributions from thermal radiation, magnetic body force, and Darcy linear impedance, the appropriate conservation equations for Magnetohydrodynamic Casson nanofluid flow emerge as:



Continuity Equation:

$$\frac{\partial u}{\partial x} + \frac{\partial v}{\partial y} = 0 \tag{2}$$

Momentum equation

$$\frac{\partial u}{\partial t} + u \frac{\partial u}{\partial x} + v \frac{\partial u}{\partial y} = \frac{\mu_{nf}}{\rho_{nf}} \left(\frac{1+\beta}{\beta} \right) \frac{\partial^2 u}{\partial y^2} - \frac{\sigma_{nf} B^2}{\rho_{nf}} u - \frac{\mu_{nf}}{\rho_{nf}} \frac{u}{K_1} \tag{3}$$

Energy equation

$$\frac{\partial T}{\partial t} + u \frac{\partial T}{\partial x} + v \frac{\partial T}{\partial y} + \lambda_1 \left(u \frac{\partial u}{\partial x} \frac{\partial T}{\partial y} + u \frac{\partial v}{\partial y} \frac{\partial T}{\partial x} + u \frac{\partial u}{\partial x} \frac{\partial T}{\partial y} + v \frac{\partial u}{\partial y} \frac{\partial T}{\partial x} + u^2 \frac{\partial^2 T}{\partial x^2} + v^2 \frac{\partial^2 T}{\partial y^2} + 2uv \frac{\partial^2 T}{\partial x \partial y} \right) = \frac{k_{nf}}{(\rho c_p)_{nf}} \frac{\partial^2 T}{\partial y^2} - \frac{1}{(\rho c_p)_{nf}} \frac{\partial q_r}{\partial y} \tag{4}$$

The proposed boundary conditions which represent physically realistic materials processing systems are prescribed as follows:

$$\left. \begin{aligned} \text{at } y = 0, v = V_w, u = U_w + W_1 \mu_{nf} (\partial u / \partial y), \\ -k_f (\partial T / \partial y) = h_f (T_w - T), \\ \text{as } y \rightarrow \infty, u, v \rightarrow 0, \&T \rightarrow T_\infty \end{aligned} \right\} \tag{5}$$

The components u and v are velocities along with the directions of x -axis and y -axis correspondingly. The thermal relaxation is represented by $\lambda_1 = \lambda_0(1 - \lambda t)$ where t is time and λ_0 is constant, $K_1 = K_0(1 - \lambda t)$ is the absorptivity of the permeable medium, $\nu_{nf} = \mu_{nf} / \rho_{nf}$ is kinematic viscosity, $W_1 = W_0 \sqrt{(1 - \lambda t)}$ is the momentum (velocity) slip factor, with W_0 initial slip parameter, $\beta = \mu_b \sqrt{2\pi c} / p_y$ is the Casson nanofluid parameter, and h_f convective heat transfer coefficient.

The radiative heat flux q_r may be specified by $q_r = -4\sigma^* / 3k^* \times \partial T / \partial y$ conferring from the Rosseland calculation, with Stefan-Boltzmann constant σ^* and k^* is the Rosseland mean absorption coefficient. This model is valid for optically thick flows. Now by substituting $\partial q_r / \partial y = 16\sigma^* T_\infty^3 / 3k^* \times (-\partial^2 T / \partial y^2)$ in Eq. (4) yields:

$$\frac{\partial T}{\partial t} + u \frac{\partial T}{\partial x} + v \frac{\partial T}{\partial y} + \lambda_1 \left(u \frac{\partial u}{\partial x} \frac{\partial T}{\partial y} + u \frac{\partial v}{\partial y} \frac{\partial T}{\partial x} + u \frac{\partial u}{\partial x} \frac{\partial T}{\partial y} + v \frac{\partial u}{\partial y} \frac{\partial T}{\partial x} + u^2 \frac{\partial^2 T}{\partial x^2} + v^2 \frac{\partial^2 T}{\partial y^2} + 2uv \frac{\partial^2 T}{\partial x \partial y} \right) = \frac{K_{nf}}{(\rho c_p)_{nf}} \frac{\partial^2 T}{\partial y^2} + \frac{1}{(\rho c_p)_{nf}} \frac{16\sigma^* T_\infty^3}{3k^*} \frac{\partial^2 T}{\partial y^2} \tag{6}$$

The material parameters of the magnetic Casson nanofluid (see Thirupathi et al. [43-47]) i.e. thermal diffusivity (α_{nf}), electrical conductivity (σ_{nf}), the heat capacitance $(\rho c_p)_{nf}$, the effective density (ρ_{nf}), the thermal conductivity (k_{nf}), and coefficient of dynamic viscosity (μ_{nf}) are given as:

$$\begin{aligned} \mu_{nf} = \mu_f (1 - \phi)^{-2.5}, \quad \alpha_{nf} = k_{nf} / (\rho c_p)_{nf}, \quad \rho_{nf} = (1 - \phi)\rho_f + \phi\rho_s, \quad \frac{(\sigma)_{nf}}{(\sigma)_f} = 1 + \frac{3((\sigma_s / \sigma_f) - 1)\phi}{((\sigma_s / \sigma_f) + 2) - ((\sigma_s / \sigma_f) - 1)\phi} \\ (\rho c_p)_{nf} = (1 - \phi)(\rho c_p)_f + \phi(\rho c_p)_s, \quad \frac{k_{nf}}{k_f} = \frac{(k_s + (m - 1)k_f) - (m - 1)\phi(k_f - k_s)}{(k_s + (m - 1)k_f) + \phi(k_f - k_s)}, \end{aligned} \tag{7}$$

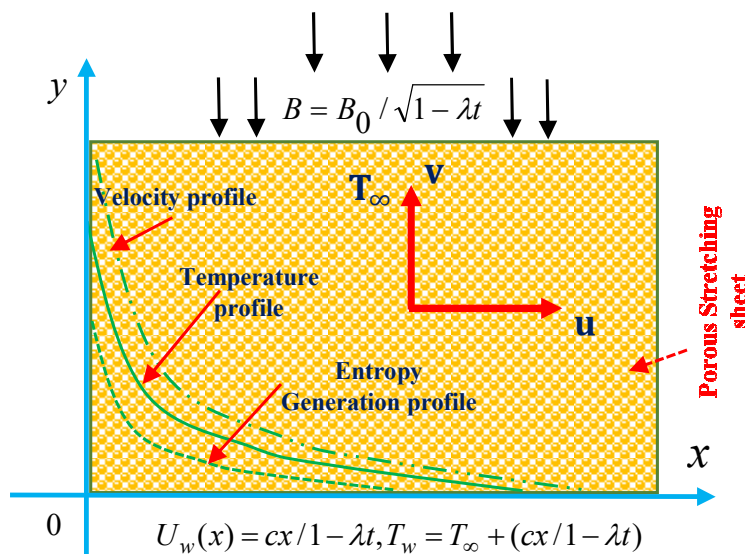


Fig. 1. Schematic of the physical model



Here ϕ is the volume fraction of nano-particle, ρ_s the density of the solid fraction, ρ_f fluid density, μ_f , the fluid viscosity, k_{nf} , k_s and k_f are the thermal conductivity of the nanofluid, solid and fluid respectively and β_f , β_s are the thermal expansion coefficients of the fluid and nanoparticles. Eqns. (2), (3) and (6) subject to the boundary conditions (5) are transformed into a coupled, non-dimensional, non-linear system of ordinary differential equations by presenting the succeeding similarity transformations (Asif et al. [20]).

$$u = \frac{\partial \psi}{\partial y}, \quad v = -\frac{\partial \psi}{\partial x}, \quad \eta = y\sqrt{c/v_f(1-\lambda t)}, \quad \psi = \sqrt{cv_f/(1-\lambda t)} xf(\eta), \quad \theta(\eta) = \frac{T-T_\infty}{T_w-T_\infty} \tag{8}$$

By substitution of Eqn. (8) to Eqns. (2), (3), (5), and (6), the non-dimensional boundary layer equations are:

$$\frac{1}{p_1 p_2} \left(1 + \frac{1}{\beta} \right) f''' + ff'' - A \left(\frac{\eta}{2} f'' + f' \right) - f'^2 - \frac{p_4}{p_2} Mf' - \frac{1}{p_1 p_2 Da} f' = 0 \tag{9}$$

$$\theta'' \left(1 + \frac{1}{p_5} Nr \right) + Pr \frac{p_3}{p_5} \left(f\theta' + A \left(\theta + \frac{\eta}{2} \theta' \right) - f'\theta - \delta(f^2\theta'' + ff'\theta') \right) = 0 \tag{10}$$

The corresponding boundary conditions take the form:

$$\begin{aligned} f(0) = S, f'(0) = 1 + \gamma \frac{1}{p_1} f''(0), \theta'(0) = -Bi(1 - \theta(0)) \\ \text{as } \eta \rightarrow \infty, f'(\eta) \rightarrow 0, \theta(\eta) \rightarrow 0 \end{aligned} \tag{11}$$

where $p_1 = (1 - \varphi)^{2.5}$, $p_2 = (1 - \varphi + \varphi(\rho_s / \rho_f))$, $p_3 = (1 - \varphi + \varphi((\rho c_p)_s / (\rho c_p)_f))$, $p_4 = (1 + [3(\sigma_s / \sigma_f - 1)\varphi] / [(\sigma_s / \sigma_f + 2) - (\sigma_s / \sigma_f - 1)\varphi])$, and $p_5 = ((k_s + (m - 1)k_f) - (m - 1)\varphi(k_f - k_s)) / [(k_s + (m - 1)k_f) + \varphi(k_f - k_s)]$,

Also f and θ are functions of η which represent stream function and temperature respectively. The dimensionless parameters arising in Eqns. (9)-(11) are $A = \lambda / c$ unsteadiness parameter, $M = \sigma_f B_o^2 / \rho_f c$ Hartmann (magnetic body force) number, $Da = k_o c / v_f$ permeability parameter, $\delta = \lambda_o c$ thermal relaxation time parameter, $\alpha_f = k_f / (\rho c_p)_f$ thermal diffusivity parameter, $Pr = (v_f / \alpha_f)$ Prandtl number, $Nr = (16 / 3)(\sigma^* T_\infty^3) / (k_f k^* v_f (\rho c_p)_f)$ radiation parameter, $S = (-V_w) \sqrt{1 - \lambda t} / cv_f$ porous wall suction/injection parameter, $Bi = \sqrt{(1 - \lambda t)v_f / c} (h_f / k_f)$ Biot number, and $\gamma = W_o \mu_f \sqrt{c / v_f}$ velocity slip parameter.

2.1 Entropy Analysis

For a magnetic Casson nanofluid, to diminish the energy wastage and to improve productivity, by following (Aziz et al. [48]), the entropy generation is defined as:

$$E_G = \frac{\mu_{nf}}{T_\infty} \left(1 + \frac{1}{\beta} \right) \left(\frac{\partial u}{\partial y} \right)^2 + \frac{\sigma_{nf} B^2}{T_\infty} u + \frac{K_{nf}}{T_\infty} \frac{\partial T}{\partial y} \left\{ \left(1 + \frac{16\sigma^* T_\infty^3}{3k^*} \right) \left(\frac{\partial T}{\partial y} \right)^2 \right\} \tag{12}$$

The non-dimensional form of the entropy generation is:

$$N_G = \frac{T_\infty^2 c^2 E_G}{k_f (T_w - T_\infty)^2} \tag{13}$$

Plugging Eq. (12) in Eq. (13) and by adopting the similarity variables in Eq. (8), we get the entropy generation number for the magnetic Casson nanofluid in dimensionless form as:

$$N_G = Re_x \left[\frac{p_5}{p_3} (\theta')^2 (1 + Nr) + \frac{1}{p_1} \frac{Br}{\Omega} \left\{ f'^2 (1 + \beta^{-1}) + p_1 p_4 Mf'^2 \right\} \right] \tag{14}$$

where $Re_x = U_w c^2 / v_f x$ is local Reynolds number, $Br = U_w \mu_f / k_f (T_w - T_\infty)$ is Brinkman number, $\Omega = (T_w - T_\infty) / T_\infty$ is a dimensionless temperature gradient. Additionally, skin friction (C_f) and local Nusselt number (Nu_x) is:

$$C_f = \frac{\tau_w}{\rho_f U_w^2}, \quad Nu_x = \frac{xq_w}{k_f (T_w - T_\infty)} \tag{15}$$

where $\tau_w = -(\mu_{nf} + p_y / \sqrt{2\pi})(\partial u / \partial y)|_{y=0}$, $q_w = -k_{nf} (1 + 16\sigma^* T_\infty^3 / 3k^* k_f)(\partial T / \partial y)_{y=0}$. Using Eq. (8) and Eq. (15) we have $Re_x^{1/2} C_f = -(1 + \beta^{-1})f''(0) / p_1$, $Re_x^{-1/2} Nu_x = -(1 + Nr)\theta'(0)k_{nf} / k_f$. Here $Re_x = xU_w / v_f$ is the local Reynolds number based on stretching velocity ($U_w(x)$).

3. ADM Solutions for the Flow Model

The set of ordinary differential equations. (9) - (10) subject to the boundary conditions (11) does not admit the exact analytical method. Therefore, numerical techniques such as finite element method, finite volume method can be useful for the computation. Now a day, semi-analytical techniques are more popular those utilizes power-series techniques with the help of symbolic codes MAPLE or MATHEMATICA for greater accuracy. To achieve faster convergence than any other method, Adomian [35] introduces a very useful polynomial approximation known as Adomian Decomposition Method (ADM). The advantage of ADM is that the analytical approximation is obtained without linearization or using the perturbation technique. Therefore, presently we have deployed ADM for the solution of the transformed equations. (9) - (10) with prescribed boundary conditions (11).

Consider an ordinary differential equation (ODE) of the form:



$$D[u(y)] = Q(y) \tag{16}$$

Here, D is the differential operator which consists of the nonlinear term $Nu(y)$ and the linear terms $(L + R)$ with L being the highest ordered derivative and easily invertible operator and R being the reminder linear part. Eqn. (16) can now be written as:

$$Lu(y) + Ru(y) + Nu(y) = Q(y) \tag{17}$$

Now the solution $u(y)$ is obtained by solving the Eqn. (17) for $Lu(y)$. Since the n^{th} order L is the highest ordered derivative and more easily invertible then L^{-1} it is the n – fold integral operator. Thus, Eqn. (17) can be written as:

$$u(y) = L^{-1}Q(y) - L^{-1}Ru(y) - L^{-1}Nu(y) \tag{18}$$

Based on Eqn. (18), the boundary layer Eqns. (9) - (10) can be written as follows:

$$f(\eta) = L_1^{-1} \left[\frac{1}{p_1 p_2 (\beta^{-1} + 1)} \left(A \left(f' + \frac{\eta}{2} f'' \right) - ff'' + f'^2 + \frac{p_4}{p_2} M f' + \frac{1}{p_1 p_2 Da} f' \right) \right] \tag{19}$$

$$\theta(\eta) = L_2^{-1} \left[\frac{1}{\left(1 + \left(\frac{1}{p_5} \right) Nr \right)} \left(Pr \frac{p_3}{p_5} \left(f \theta' - f' \theta + A \left(\theta + \frac{\eta}{2} \theta' \right) - \delta (f^2 \theta'' + ff' \theta') \right) \right) \right] \tag{20}$$

Here L_1 & L_2 designate the 3rd and 2nd order differential operators $L_1 = d^3(*) / d\eta^3$ and $L_2 = d^2(*) / d\eta^2$, respectively. Consequently, L_1^{-1} & L_2^{-1} denote the 3 – fold & 2 – fold indefinite the following integral operators:

$$L_1^{-1}(*) = \int_0^\eta \int_0^\eta \int_0^\eta (*) d\eta_1 d\eta_2 d\eta_3 \text{ and } L_2^{-1}(*) = \int_0^\eta \int_0^\eta (*) d\eta_1 d\eta_2$$

respectively. Furthermore, the constants of integration L_1^{-1} & L_2^{-1} are computed from the given initial and boundary conditions. In ADM, the analytical approximate solutions to nonlinear equations are obtained without linearization and discretization. Therefore, to get more realistic results, ADM assumes the solution $u(y)$ as an infinite series:

$$u(y) = \sum_{n=0}^{\infty} u_n \tag{21}$$

Now the unknown solutions $f(\eta)$ & $\theta(\eta)$ can be expressed respectively as:

$$f(\eta) = \sum_{n=0}^{\infty} f_n(\eta) \text{ \& } \theta(\eta) = \sum_{n=0}^{\infty} \theta_n(\eta) \tag{22}$$

Finally, the non-linear term $Nu(y)$ is assumed to analytic and writing as an infinite series, we have:

$$Nu(y) = \sum_{n=0}^{\infty} A_n \tag{23}$$

Here A_n represents specially generated Adomian polynomials. The linear and nonlinear terms of (19) - (20) can be expressed in the form of polynomials as:

$$\left. \begin{aligned} \sum_{m=0}^{\infty} A_m &= f', \sum_{m=0}^{\infty} B_m = f'', \sum_{m=0}^{\infty} C_m = ff'', \sum_{m=0}^{\infty} D_m = f'^2, \sum_{m=0}^{\infty} E_m = f \theta', \\ \sum_{m=0}^{\infty} F_m &= f' \theta, \sum_{m=0}^{\infty} G_m = \theta, \sum_{m=0}^{\infty} H_m = \theta', \sum_{m=0}^{\infty} I_m = f^2 \theta'', \sum_{m=0}^{\infty} J_m = ff' \theta' \end{aligned} \right\} \tag{24}$$

The components of $u(y)$ say $u_n(y), n = 0, 1, 2, \dots$ are computed for specified values of A_n . Therefore, Eqn. (23) can be written as:

$$u_{n+1}(y) = \sum_{n=0}^m A_n \tag{25}$$

Now, the recursive relations for the present problem are given by:

$$f_{m+1}(\eta) = L_1^{-1} \left[\frac{1}{p_1 p_2 (\beta^{-1} + 1)} \left(A \left(A_m + \frac{\eta}{2} B_m \right) - C_m + D_m + \frac{p_4}{p_2} M A_m + \frac{1}{p_1 p_2 Da} A_m \right) \right] \tag{26}$$

$$\theta_{m+1}(\eta) = L_2^{-1} \left[\frac{1}{\left(1 + \left(\frac{1}{p_5} \right) Nr \right)} \left(Pr \frac{p_3}{p_5} \left(E_m - F_m + A \left(G_m + \frac{\eta}{2} H_m \right) - \delta (I_m + J_m) \right) \right) \right] \tag{27}$$



Table 1. The thermo-physical values of nano-sized materials and water

	H ₂ O (See [50,51])	Cu (See [50,51])	CuO (See [52])
(kg/m ³) ρ	997.1	8933	6500
(J kg ⁻¹ K ⁻¹) c _p	4179	385	540
(W m ⁻¹ K ⁻¹) k	0.613	401	18
(10 ⁻⁵ K ⁻¹) × β	21	1.67	1.8
(Ω ⁻¹ m ⁻¹) σ	0.05	5.96×10 ⁷	2.7×10 ⁻⁸

Using assumed initial guess solutions:

$$f_0(\eta) = S + \eta \left(1 + \frac{\gamma p}{p_1} \right) + \frac{1}{2} p \eta^2 \tag{28}$$

$$\theta_0(\eta) = 1 + \left(\frac{1}{Bi} + \eta \right) q \tag{29}$$

The approximated analytical solutions are given by:

$$f(\eta) = \sum_{k=0}^n f_k(\eta) \tag{30}$$

$$\theta(\eta) = \sum_{k=0}^n \theta_k(\eta)$$

The unknown assumed values $p = f''(0)$ and $q = \theta'(0)$ are obtained numerically and given in Table 2. The methodology employed in this article is explained by the authors comprehensively in Thirupathi et al. [49].

4. Validation, Results, and Discussion

Extensive ADM solutions have been derived and visualized. Both metal (Copper-Cu) and metallic oxide (Copper oxide-CuO) are taken into consideration as the nanoparticles with water as a base fluid. Table 1 summarizes the thermo physical properties of various nanoparticles based on the Tiwari-Das-Maxwell model along with the base fluid water properties. The semi-analytical method used for the solution of the nonlinear coupled equation requires the unknown boundary conditions such as $f''(0) = p$ & $\theta'(0) = q$. At the time of computation, these values are obtained using the shooting technique for variation of contributing parameters as shown in Table 2. Further details are given in [50] - [52]. Here, the unknowns are computed for magnetic Cu-water and CuO-water nanofluids.

The velocity and temperature profiles with variation in the emerging control parameters are presented in Figs. 2-18. For the validation of the ADM solutions, the comparison is conducted with the non-permeable ($Da = \infty$) case with $\beta = 0, Bi \rightarrow \infty$ as studied earlier by Asif et al. [20] and Das et al. [53] and shown in Table 3. An excellent agreement is obtained confirming the accuracy of the ADM solutions.

4.1 Velocity distribution

Fig. 2 shows the impact of nanoparticle volume fraction on velocity contours for both the Cu and CuO-water nanofluids. Here, the case of pure fluid ($\phi = 0$) is also considered for further verification of the ADM solutions. For $\phi = 0$, the present solutions concur with Asif et al. [20]. However, with an increasing nanoparticle volume fraction, the velocity decreases i.e. the nanofluid flow decelerates near the sheet whereas far away from the sheet the effect is reversed. It is observed that the velocity of Cu-water nanofluid decreases more than CuO-water nanofluid. This is probably attributable to a heavier density; Cu nanoparticles are clogged near the wall which retards the velocity profiles throughout the boundary layer.

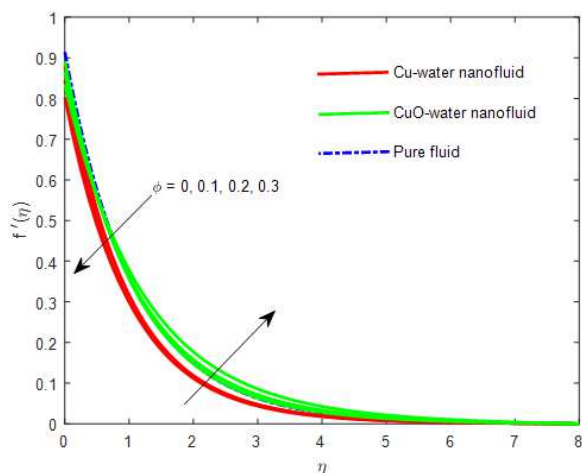


Fig. 2. Variation of $f'(\eta)$ for ϕ

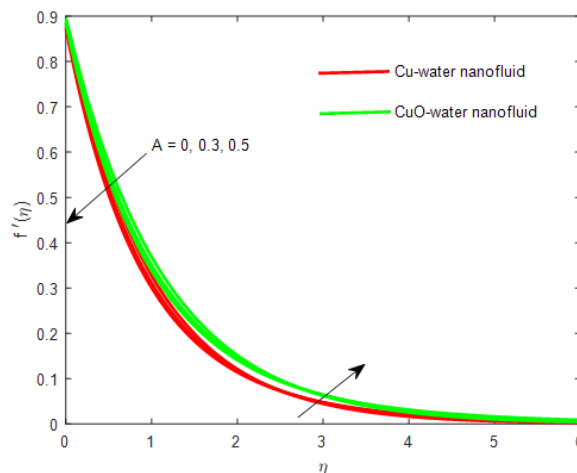


Fig. 3. Variation of $f'(\eta)$ for A



Table 2. Approximate unknown values

ϕ	Cu – H ₂ O		CuO – H ₂ O	
	p	q	p	q
0	-0.85806	-0.18546	-0.85806	-0.18546
0.1	-0.91936	-0.18182	-0.83386	-0.1825
0.2	-0.89186	-0.17668	-0.76936	-0.17853
0.3	-0.80806	-0.16833	-0.67616	-0.17269
A				
0	-0.8817	-0.18288	-0.79673	-0.18347
0.3	-0.93773	-0.18123	-0.85198	-0.18196
0.5	-0.97353	-0.17988	-0.88726	-0.18074
β				
2	-1.04226	-0.18128	-0.9468	-0.18205
5	-1.14705	-0.18078	-1.04337	-0.18163
10	-1.19025	-0.18055	-1.08326	-0.18145
M				
0.1	-0.81568	-0.18225	-0.75899	-0.18278
0.6	-0.91936	-0.18182	-0.83386	-0.1825
1.6	-1.08752	-0.18105	-0.96067	-0.18198
Da				
10	-0.93592	-0.18175	-0.85277	-0.18243
1	-1.08246	-0.18108	-1.01626	-0.18174
0.5	-1.21652	-0.18039	-1.16163	-0.18106
Nr				
0.1	-1.216519	-0.181739	-1.16163	-0.182387
0.3	-1.216519	-0.180389	-1.16163	-0.181056
0.5	-1.216519	-0.179094	-1.16163	-0.179783
γ				
0.1	-1.216519	-0.180389	-1.16163	-0.181056
0.2	-1.035707	-0.178846	-0.99586	-0.179646
0.4	-0.803259	-0.176035	-0.77914	-0.177077
Bi				
0.1	-1.216519	-0.094845	-1.16163	-0.095029
0.2	-1.216519	-0.180389	-1.16163	-0.181056
0.3	-1.216519	-0.257938	-1.16163	-0.259304
δ				
0.01	-1.216519	-0.180389	-1.16163	-0.181056
0.2	-1.216519	-0.180826	-1.16163	-0.18148
0.4	-1.216519	-0.181285	-1.16163	-0.181928

Table 3. Comparison of results for several values of Pr whenever $\beta = 0, Bi \rightarrow \infty$

Pr	Das et al. [53]	$Nu_x Re_x^{-1/2}$	Asif et al. [20]	$Nu_x Re_x^{-1/2}$	Present results	$Nu_x Re_x^{-1/2}$
0.72	0.80876122		0.80876181		0.80876201	
3.0	1.92357431		1.92357420		1.92357399	
7.0	3.07314679		3.07314651		3.07314712	
10	3.72055436		3.72055424		3.72055536	

Fig. 3 describes the behavior of the unsteadiness parameter on the velocity profiles for the fixed values of other parameters. Here, $A = 0$ and it corresponds to steady-state behavior and $A \neq 0$ is associated with the unsteady state. It is apparent that the steady-state velocity is maximum near the sheet and further with an increase in unsteadiness the profile decreases rapidly up to the region $\eta < 2.6$ (approximately) where a point of inflection of the profiles is observed. Thereafter a slight increase in the profile is present and profiles asymptotically tend to the imposed boundary condition. Concerning Cu-water and CuO-water nanofluids, it is observed that the velocity of Cu-water nanofluid decreases significantly.

The impact of the magnetic body force parameter on the velocity distribution of both the nanofluids is exhibited in Fig. 4. The effect is quite general. The profile of velocity is suppressed for all locations with the increasing magnetic field and therefore momentum boundary layer thickness is decreased. The magnetic nanofluid is subjected to increasing Lorentzian impedance which inhibits the momentum development and decelerates the flow. Vanishing magnetic field ($M = 0$ i.e. the nanofluid is electrically non-conducting in this case) manifests in the optimal conditions for flow and results in maximum velocity. However, for enhanced flow control in materials processing operations, the presence and manipulation of a transverse magnetic field achieves the desired effect and suppresses velocities i.e. damps the boundary layer flow. This permits more homogenous constitutions of manufactured materials to be obtained as noted by Asai [54]. However, Cu-water nanofluid achieves markedly lower velocity magnitudes in comparison to CuO-water nanofluid.

Fig. 5 designates the impact of Darcy number on the velocity field. Darcy linear body force is inversely proportional to Darcy number and therefore with higher Da values, there is a strong acceleration in the flow (and a corresponding depletion in Darcy drag). The porous medium, therefore, acts similarly to the magnetic field. Porosity, a resistive force that resists the fluid motion in conjunction with the magnetic parameter. Lower permeability porous media achieve significant damping of the nanofluid velocity resulted in the retardation in the profiles exhibited. The behavior of Cu-water nanofluid is similar to the description of Fig. 4 presented earlier.



Table 4. Computation of $C_f Re_x^{1/2}$ and $Nu_x Re_x^{-1/2}$ for different parameter values

ϕ	A	β	M	Da	Nr	γ	Bi	δ	Cu – H ₂ O		CuO – H ₂ O	
									$C_f Re_x^{1/2}$	$Nu_x Re_x^{-1/2}$	$C_f Re_x^{1/2}$	$Nu_x Re_x^{-1/2}$
0	0.2	1	0.6	100	0.3	0.1	0.2	0.01	-1.716128	0.2411024	-1.716128	0.2411024
0.1									-2.392805	0.2182555	-2.170278	0.2204774
0.2									-3.116014	0.1994903	-2.688025	0.2036346
0.3									-3.942099	0.181059	-3.298654	0.188053
0.1	0								-2.294791	0.2195219	-2.073639	0.2216442
	0.3								-2.44064	0.2175422	-2.217452	0.2198242
	0.5								-2.533799	0.2159211	-2.30928	0.2183498
	0.2	2							-2.034523	0.217605	-1.84818	0.2199347
		5							-1.791257	0.2169993	-1.629347	0.2194332
		10							-1.703827	0.2167344	-1.550663	0.2192151
		1	0.1						-2.122971	0.2187665	-1.97541	0.2208181
			0.6						-2.392805	0.2182555	-2.170278	0.2204774
			1.6						-2.830488	0.217334	-2.50033	0.2198554
			0.6	10					-2.435927	0.21817	-2.219503	0.2203884
				1					-2.817311	0.2173636	-2.645012	0.2195631
				0.5					-3.166231	0.216536	-3.023369	0.2187341
				0.5	0.1				-3.166231	0.1938784	-3.023369	0.1950386
					0.3				-3.166231	0.216536	-3.023369	0.2187341
					0.5				-3.166231	0.2389054	-3.023369	0.2421383
					0.3	0.1			-3.166231	0.216536	-3.023369	0.2187341
						0.2			-2.695633	0.2146833	-2.591918	0.2170299
						0.4			-2.090639	0.2113089	-2.027869	0.2139261
						0.1	0.1		-3.166231	0.1138497	-3.023369	0.1148041
							0.2		-3.166231	0.216536	-3.023369	0.2187341
							0.3		-3.166231	0.3096242	-3.023369	0.3132652
							0.2	0.01	-3.166231	0.216536	-3.023369	0.2187341
								0.2	-3.166231	0.2170596	-3.023369	0.2192464
								0.4	-3.166231	0.2176116	-3.023369	0.2197877

Fig. 6 portrays the influence of momentum (velocity) slip parameter, γ on the velocity profile for fixed values of the other parameters. It is interesting to observe that an increasing slip decreases the velocity magnitude for both magnetic nanofluids. Hydrodynamic slip at the wall implies a non-adherence of the boundary layer there. There is a delay incurred in the momentum diffusion in the near-wall region and this leads to a thickening of the momentum boundary layer and concomitant deceleration in the flow. The amount of retardation is greater with higher slip in conjunction with the opposite force i.e. the magnetic body force. Further, it exacerbates the retardation in the profile. Furthermore, in comparison to both the nanofluids, Cu-water nanofluid exhibits greater retardation throughout the boundary layer due to its higher density.

4.2 Temperature distribution

The impact of nano-sized particle volume fraction on the temperature profiles of Cu-water and CuO-water nanofluid is depicted in Fig. 7. In the case of pure fluid ($\phi = 0$) the temperature profile is suppressed which coincides with the result of Asif et al. [20]. However, with an increase in volume fraction, there is a significant increase in nanofluid temperature and thermal boundary layer thickness is elevated. It is also observed that the Cu-water nanofluid temperature has a dominating behavior over the CuO-water nanofluid. Although Cu-water has the maximum density considered in the simulations, the superior thermal conductivity encourages thermal diffusion which boosts the temperatures. The heavier density that resists the velocity distribution near the sheet region, the stored energy gives up for which the temperature profiles overshoots, and as a result fluid temperature enhances.

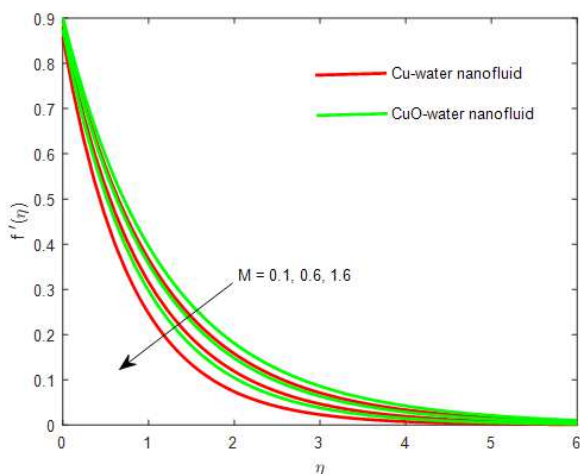


Fig. 4. Variation of $f'(\eta)$ for M

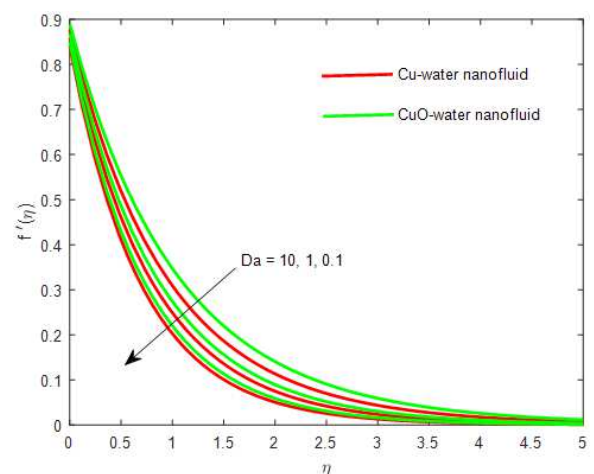


Fig. 5. Variation of $f'(\eta)$ for Da



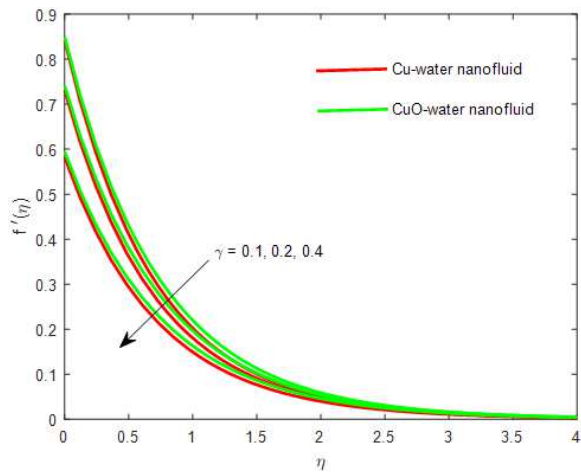


Fig. 6. Variation of $f'(\eta)$ for γ

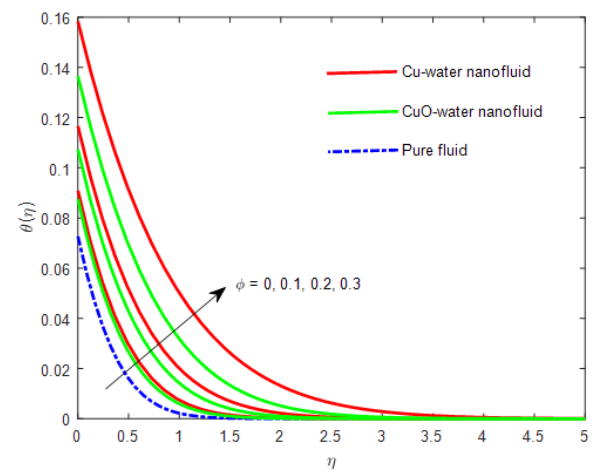


Fig. 7. Variation of $\theta(\eta)$ for ϕ

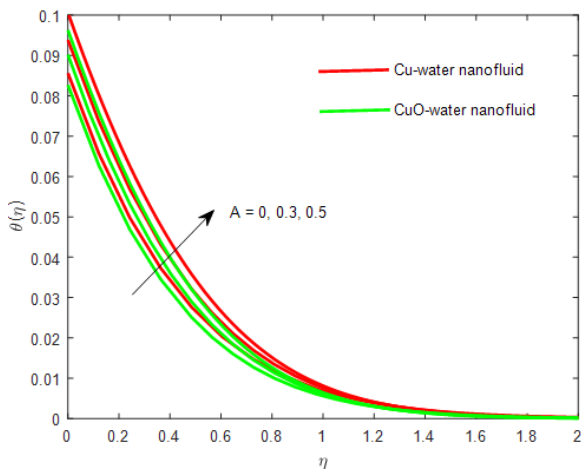


Fig. 8. Variation of $\theta(\eta)$ for A

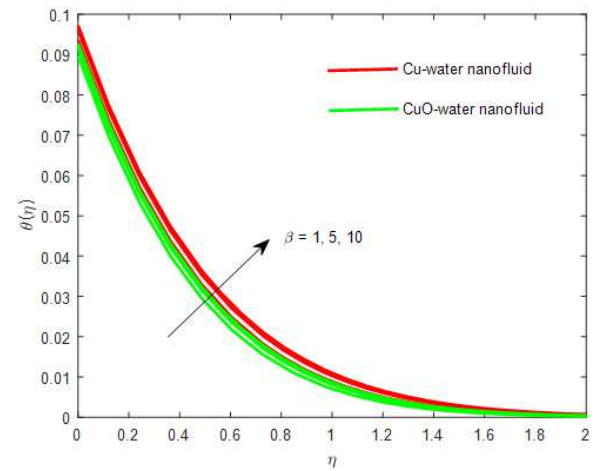


Fig. 9. Variation of $\theta(\eta)$ for β

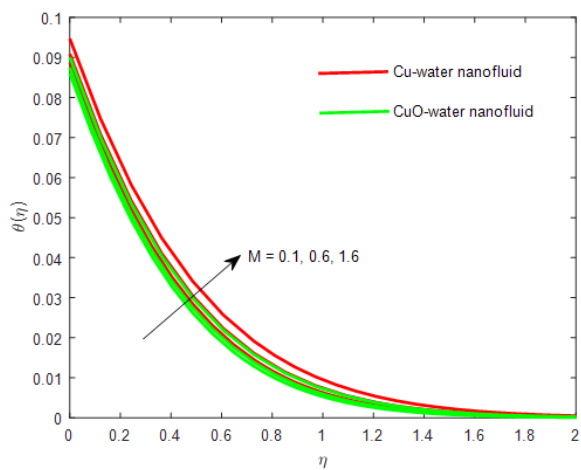


Fig. 10. Variation of $\theta(\eta)$ for M

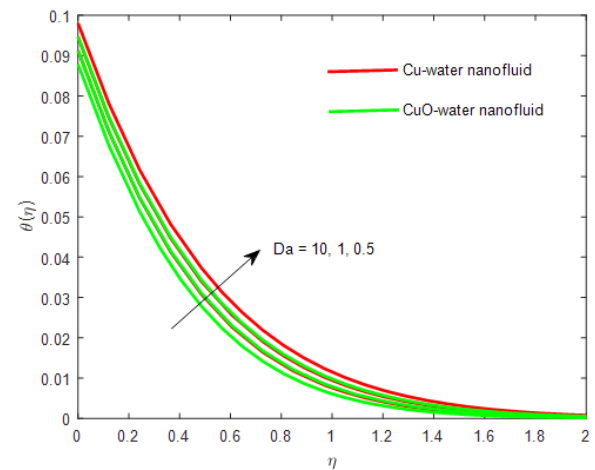


Fig. 11. Variation of $\theta(\eta)$ for Da

Fig. 8 portrays the influence of unsteadiness parameter on the temperature profiles of both the magnetic nanofluids. In the case of steady-state flow, the temperature of the nanofluids attains their minimum value close to the wall. However, greater unsteadiness increases the fluid temperature resulting in a thickening of the thermal boundary layer. Cu-water nanofluids achieve markedly greater temperatures than CuO-water nanofluids. A sharp decrease in all the profiles is observed up to the region $\eta < 0.8$ and further, it decreases smoothly following the boundary conditions.

The impact of the Casson (viscoplastic) parameter, β on the fluid temperature is shown in Fig. 9. The non-Newtonian character plays a vital role in modifying the nanofluid temperature. Elevation in the Casson parameter encourages thermal diffusion and heats the nanofluid. Throughout the thermal boundary layer, the Cu-water nanofluid temperature dominates over the CuO-water nanofluid temperature. Due to the greater thermal conductivity of the copper metal in comparison to CuO, such a



situation is noticed in the thermal boundary layer.

Fig. 10 describes the influence of the magnetic body force parameter (modified Hartmann number, $M = \sigma_f B_o^2 / \rho_f c$) on the temperature contours for both the nanofluids. The nanofluid has to expend extra work to move against the action of the Lorentz drag force. This kinetic energy is dissipated as heat in the nanofluid and temperature is therefore enhanced significantly. Moreover, for a higher value of the magnetic parameter, the maximum temperature is rendered in the case of Cu-water nanofluid in the entire domain.

Fig. 11 visualizes the effect of Darcy number, Da , on the temperature profiles. With increasing Da values there is a prominent reduction in temperatures. The progressive decrease in solid fibers in the permeable medium with larger Darcy number (i.e. higher permeability) results in suppression in thermal conduction heat transfer. This cools off the regime and reduces thermal boundary layer thickness. Again, higher temperatures are calculated for Cu-water nanofluid compared with CuO-water nanofluid throughout the domain.

The effect of the thermal radiation parameter, Nr , on the temperature profile of Casson nanofluid is presented in Fig. 12. $Nr = (16/3)(\sigma^* T_\infty^3) / (k_f k^* v_f (\rho c_p)_f)$ and expresses the relative contribution of thermal radiative heat transfer and thermal conduction heat transfer. The present case simulates for various values of radiative heat energy. For $Nr = 1$ both the modes contribute equally however, for $Nr > 1$ thermal radiation dominates over the thermal conduction and for $Nr < 1$, thermal conduction dominates. Increasing Nr values elevate the temperature since with greater radiative flux the nanofluid is energized and thermal boundary layer thickness is also increased. However, again copper nanoparticles attain higher temperatures than copper oxide nanoparticles in combination with water.

The influence of velocity slip on temperature evolution for both nanofluids is displayed in Fig. 13. Velocity slip is known to decelerate the flow i.e. inhibits momentum diffusion. However, with fixed Prandtl number (which expresses the ratio of momentum and thermal diffusivities) the thermal diffusion is assisted, and this leads to heating of the boundary layer and elevation in temperatures.

Fig. 14 represents the influence of thermal Biot number, Bi , on the temperature contour for fixed values of the other parameters. $Bi = (h_f / k_f) \sqrt{v_f (1 - \lambda t)} / c$ and arises in the thermal wall boundary condition (11). It quantifies the relative importance of thermal conduction and thermal convection at the surface. It is, therefore, a key parameter employed in materials processing for determining the temperature history of a body being heated or cooled by convection at its surface. Which $Bi < 0.1$ and for which it is seldom necessary to solve the conduction equation, i.e., convection is the rate-controlling process. In the computations considered herein, Bi is greater than or equal to 0.1, and the regime is defined as thermally thick (the case for $Bi < 0.1$ i.e. thermally thin is not relevant here). Greater Bi values imply enhanced thermal conduction relative to convection at the wall and this results in a boost in nanofluid temperature and greater thermal boundary layer thickness.

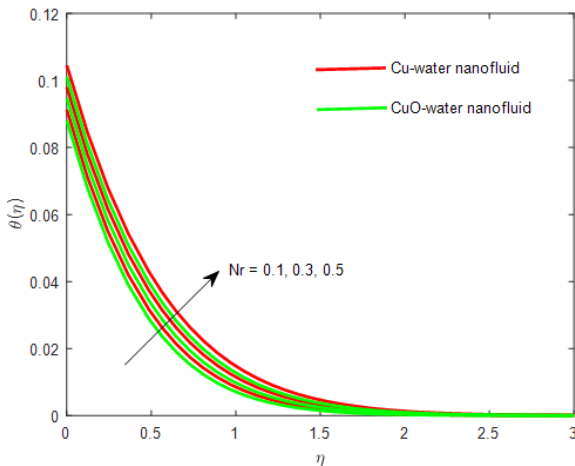


Fig. 12. Variation of $\theta(\eta)$ for Nr

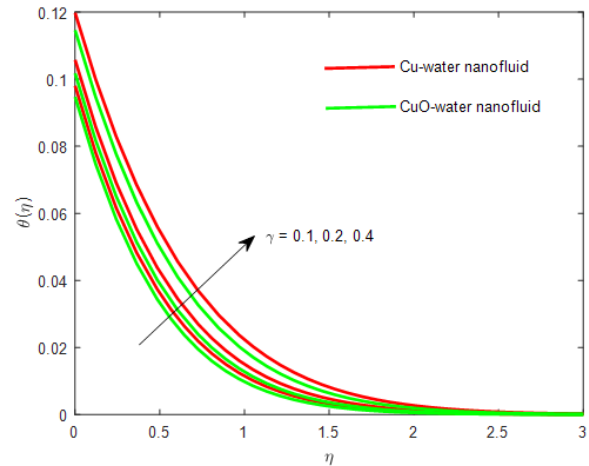


Fig. 13. Variation of $\theta(\eta)$ for γ

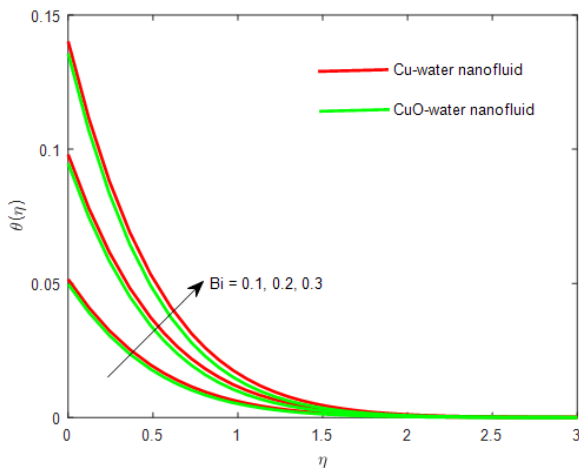


Fig. 14. Variation of $\theta(\eta)$ for Bi

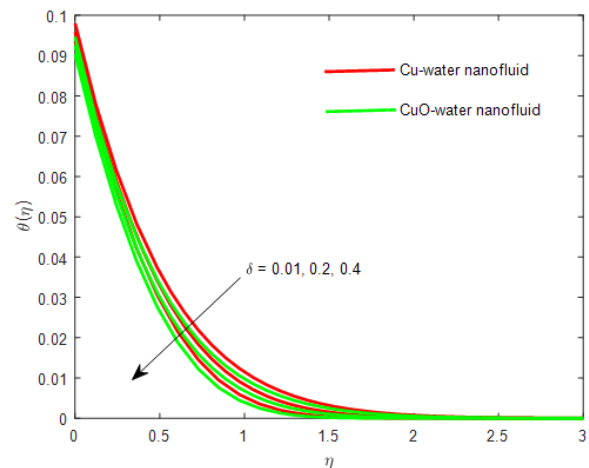


Fig. 15. Variation of $\theta(\eta)$ for δ



Fig. 15 pronounces the deviation of temperature profiles for diverse values of thermal relaxation time parameter ($\delta = \lambda_0 c$). Significant depletion in temperature is associated with greater relaxation times. The implication is that with conventional Fourier models (vanishing δ) temperatures are over-estimated and errors are incurred. The non-Fourier model corrects this by computing lower temperatures with greater thermal relaxation time. Moreover, it is evident that copper nanofluid consistently attains higher temperatures than copper oxide nanofluid with water as a base fluid, irrespective of the thermal relaxation time.

4.3 Entropy generation

The amount of entropy encountered in any of the irreversibility processes is the so-called entropy generation. The irreversibility is higher due to higher entropy generation and that causes the lower efficiency of the device. Therefore, the influence of nanofluid volume fraction, Brinkman number, and temperature gradient parameter on entropy generation is portrayed in Figs. 16-18. From the figures, it is witnessed that enhancing the volume fraction of nanoparticle (see Fig. 16) and Brinkman number (see Fig. 17), leads to an elevation in magnitudes of entropy generation. Since viscous heating is greater than the thermal energy transfers due to molecular diffusivity, there is a boost in entropy production. However, the opposite behavior is observed with the temperature gradient (see Fig. 18) parameter which induces a strong depression in entropy generation. In all cases copper water nanofluid attains the highest entropy generation, then copper oxide nanofluid, and finally the lowest values are associated with pure water.

Based on the velocity and temperature functions, the skin friction and local Nusselt number can be computed. Table 4 shows these values for both nanofluids. Increasing nanoparticle volume fraction elevates the skin friction (shear stress) for both the nanofluids whereas it depletes the local Nusselt number i.e. surface rate of heat transfer. Volume fraction has a more prominent impact on Cu-water nanofluid friction factor and local Nusselt number than for CuO-water nanofluid. In the steady-state scenario, the skin friction is minimum whereas in the unsteady state skin friction is enhanced. However, the rate of heat transfers i.e. the local Nusselt number for both the nanofluids decreases slightly from the steady-state to the unsteady state cases. Moreover, the opposite effect is seen in the case of increasing the Casson viscoplastic parameter. Both the resistive forces i.e. magnetic Lorentz body force and Darcy drag force decrease the skin friction for both nanofluids whereas the impact on the local Nusselt number is insignificant. Elevation in the thermal radiation parameter depresses the surface heat transfer rate. Skin friction is greater for CuO nanoparticles compared with Cu. Increasing velocity slip reduces the skin friction whereas with an upsurge in thermal Biot number the local Nusselt number is enhanced. Finally, an increase in the thermal relaxation time parameter ($\delta = \lambda_0 c$) marginally modifies the local Nusselt number. From the above discussion, it is concluded that Cu-water achieves the best thermal enhancement.

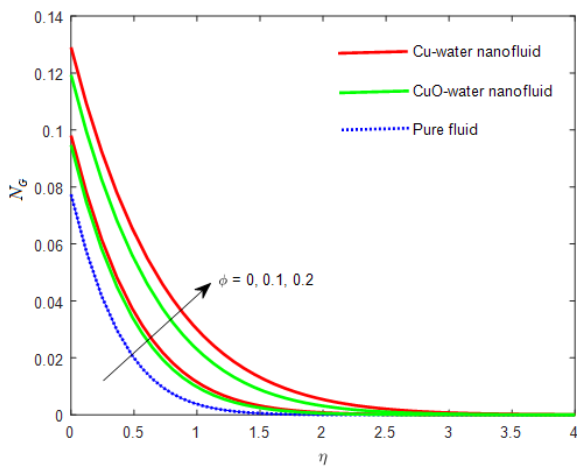


Fig. 16. Variation of N_c for ϕ

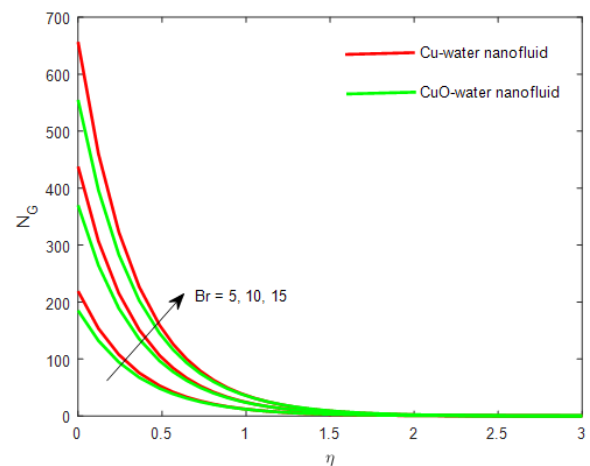


Fig. 17. Variation of N_c for Br

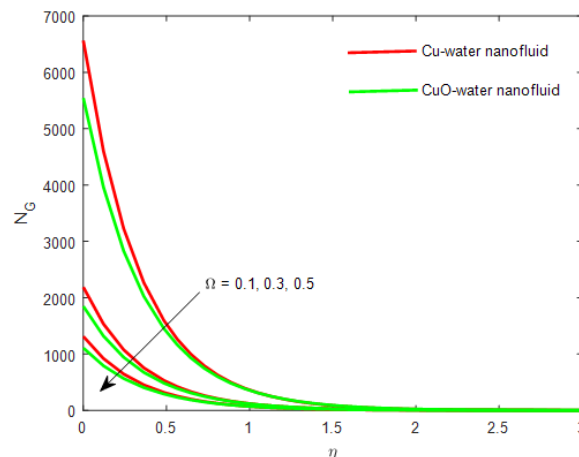


Fig. 18. Variation of N_c for Ω



5. Conclusions

In the current article, the Cattaneo-Christov heat flux model has been used to simulate thermal relaxation in unsteady hydromagnetic Casson nanofluid flow from a stretching sheet in a porous medium with thermal radiation and viscous dissipation. The model has been developed to analyze manufacturing processes for magnetic nano liquids. Both copper and copper oxide metallic nanoparticles with water base fluid have been studied using the Tiwari-Das-Maxwell formulation. The Adomian Decomposition Method (ADM) is employed for solving the transformed momentum and thermal boundary layer equations subject to velocity slip and convective temperature boundary conditions. Verification of the ADM solutions with published literature has been included. The key observations of the present simulations are summarized below:

- Nanofluid velocity magnitudes decrease with increasing values of the magnetic field, velocity slip, volume fraction, unsteadiness parameter, and Darcy number. However, velocity contours exhibit different behavior (flow acceleration) with unsteadiness and volume fraction parameter at the free-stream boundary.
- The temperature of the nanofluid is augmented with increasing magnetic field, volume fraction, unsteadiness, thermal radiation, velocity slip, Casson viscoplastic parameter, and Darcy and Biot numbers. However, temperature (and thermal boundary layer thickness) is reduced with increasing non-Fourier (thermal relaxation) parameter. The entropy contours are elevated with increasing nanoparticle volume fraction and Brinkman number whereas they are suppressed with greater values of temperature gradient parameter.
- The numerical values of friction factor and local Nusselt number decrease with greater values of volume fraction, unsteadiness, and magnetic field parameter, although the reverse trend is observed with increasing Darcy number. However, skin friction values are increased and local Nusselt number values are decreased with greater Casson viscoplastic and velocity slip parameters. Increasing radiation parameter, Biot number, and thermal relaxation parameter exert a minimal effect on the skin friction factor whereas they are found to noticeably modify the local Nusselt number.
- Greater velocities are computed for CuO-water nanofluid than Cu-water nanofluid, while the opposite behavior is computed for the case of temperature distributions.

The present study has neglected Hall Current effects (Bég et al. [55]). These also constitute important aspects of Magnetohydrodynamic nanomaterials processing and will be considered in the future. The authors are also anticipating to improve the current fluidic model on various boundary conditions on wavy and rough surfaces by considering the Corciones experimental correlations for the operative thermal conductivity and viscosity of nanofluid flows. For the higher level of numerical treatment of the current investigation, the advanced numerical approaches, such as SLLM (Spectral Local-Linearization Method (See [56])), (GDQM) (See [57]) Generalized Differential Quadrature Method will be employed.

Acknowledgments

The authors are thankful to all reviewers for their insightful comments on our research paper which led to improvements in the quality of the paper scientifically.

Conflict of Interest

The authors declared no potential conflicts of interest with respect to the research, authorship and publication of this article.

Funding

The authors received no financial support for the research, authorship and publication of this article.

Nomenclature

(x, y)	Coordinate system
(u, v)	Velocities along coordinate axes
B_0	Strength of the magnetic field
B	Magnetic field
$U_w(x), V_w(x)$	Dimensional Velocities along coordinate axes
T	Dimensional Temperature of the fluid
T_w	Temperature at surface
T_∞	Temperature at free stream
t	Time
p_y	Yield stress
e_{ij}	Component of the deformation rate
k_{nf}	Thermal conductivity of nanofluid
k_s	Thermal conductivity of solid
k_f	Thermal conductivity of the fluid
c_p	Specific heat
k'	Rosseland mean absorption coefficient
h_f	Convective heat transfer coefficient
W_1	Momentum slip parameter
W_0	Initial slip parameter
A	Unsteadiness parameter
M	Hartmann number



$f(\eta)$	Momentum function
$\theta(\eta)$	Temperature function
Nr	Radiation parameter
Pr	Prandtl number
Da	Permeability parameter
S	Suction/Injection parameter
Bi	Biot number
E_G	Dimensional Entropy generation parameter
N_G	Dimensionless Entropy generation
Re_x	Local Reynolds number
Br	Brinkman number
C_f	Skin friction
Nu_x	Local Nusselt number
q_w	Wall heat flux
D	Differential Operator
L	Linear Operator
R	Reminder of Linear Part
N	Non-Linear Part
Q	Non-homogeneous function
L^{-1}	n-fold integral operator
A_n	Adomian polynomials

Greek symbols

η	Similarity variable
τ_{ij}	Stress tensor
ϕ	Volume fraction parameter
π	Product of the deformation rate
π_c	Critical value of the product
ρ_{nf}	Density of nanofluid
ρ_s	Density of solid
ρ_f	Density of fluid
$(\rho c_p)_{nf}$	Heat capacitance of nanofluid
σ_{nf}	Electrical conductivity of nanofluid
σ_s	Electrical conductivity of solid
σ_f	Electrical conductivity of the fluid
γ	Slip parameter
Ω	Dimensionless gradient
τ_w	Wall skin friction
λ, λ_0	Constants
λ_1	Thermal relaxation parameter
ν_{nf}	Kinematic viscosity of nanofluid
β	Casson fluid parameter
μ_B	Plastic viscosity
β_s	Thermal expansion coefficient of solid
β_f	Thermal expansion coefficient of fluid
α_{nf}	Thermal diffusivity of nanofluid
μ_{nf}	Dynamic viscosity of nanofluid
μ_f	Dynamic viscosity of the fluid
σ^*	Stefan-Boltzmann constant
ψ	Stream function
δ	Dimensionless thermal relaxation parameter

Subscripts

w	wall condition
f	fluid
s	solid
nf	nanofluid
n	degree of Adomian polynomial
∞	free stream condition



References

- [1] Choi, S.U.S., Enhancing thermal conductivity of fluids with nanoparticles. In: Siginer DA and Wang HP (Eds.), *Developments and Applications of Non-Newtonian Flows*, ASME, New York, 66, 1995, 99-105.
- [2] Buongiorno, J., Convective transport in nanofluids, *ASME J Heat Transfer*, 128, 2006, 240-250.
- [3] Khan, MD. I., Qayyum, S., Hayat, T., Waqas, MD., Imran Khan, MD., and Alsaedi, A., Entropy generation minimization and binary chemical reaction with Arrhenius activation energy in MHD radiative flow of nanomaterial, *Journal of Molecular Liquids*, 259, 2018, 274-283.
- [4] Zohra, F.T., Uddin, M.J., Ismail, A.I., and Bég, O. Anwar., Bioconvective electromagnetic nanofluid transport from a wedge geometry: simulation of smart electro-conductive bio-nano-polymer processing, *Heat Transfer-Asian Res.*, 47, 2018, 231-250.
- [5] Khan, MD. I., Qayyum, S., Hayat, T., Imran Khan, MD., Alsaedi, A., and Khan, T.A., Entropy generation in radiative motion of tangent hyperbolic nanofluid in presence of activation energy and nonlinear mixed convection, *Physics Letters A*, 382(31), 2018, 2017-2026.
- [6] Prakash, J., Siva, E.P., Tripathi, D., Kuharat, S., and Bég, O. Anwar., Peristaltic pumping of magnetic nanofluids with thermal radiation and temperature-dependent viscosity effects: modelling a solar magneto-biomimetic nano pump, *Renewable Energy*, 133, 2019, 1308-1326.
- [7] Li, Z., Asadi, S., Karimipour, A., Abdollahi, A., and Tlili, I., Experimental study of temperature and mass fraction effects on thermal conductivity and dynamic viscosity of SiO₂-oleic acid/liquid paraffin nanofluid, *International Communications in Heat and Mass Transfer*, 110, 2020, 104436.
- [8] Kumar, M., Reddy, G. J., Kumar, N. N., and Bég, O. Anwar., Computational study of unsteady couple stress magnetic nanofluid flow from a stretching sheet with Ohmic dissipation, *Proc. IMechE-Part N: J Nanoengineering, Nanomaterials and Nano-systems*, 233(2-4), 2019, 49-63.
- [9] Ray, A.K., Vasu, B., Bég, O.A., Gorla, R.S.R., and Murthy, P.V.S.N., Magneto-bioconvection flow of a Casson thin film with nanoparticles over an unsteady stretching sheet: HAM and GDQ computation, *Int. J. Numerical Methods Heat Fluid Flow*, 29(11), 2019, 4277-4309.
- [10] Ngiangia, A.T., and Akaezue, N.N., Heat transfer of mixed convection electro conductivity flow of copper nanofluid with different shapes in a porous microchannel provoked by radiation and first order chemical reaction, *Asian J. of Physical and Chemical Sciences*, 7(1), 2019, 1-14.
- [11] Li, Z., Amin S., Al-Rashed, A.A.A.A., and Talebizadehsardari, P., Effect of porous medium and nanoparticles presences in a counter-current triple-tube composite porous/nano-PCM system, *Applied Thermal Engineering*, 167, 2020, 114777
- [12] Ma, X., Sheikholeslami, M., Jafaryar, M., Shafee, A., Nguyen-Thoi, T., and Li, Z., Solidification inside a clean energy storage unit utilizing phase change material with copper oxide nanoparticles, *Journal of Cleaner Production*, 245, 2020, 118888.
- [13] Bhatti, M.M., Abbas, T., Rashidi, M.M., and Ali, M.E.S., Numerical Simulation of Entropy Generation with Thermal Radiation on MHD Carreau Nanofluid towards a Shrinking Sheet, *Entropy*, 18, 2016, 200.
- [14] Fourier, J.B.J., *Theorie analytique de la chaleur*, Didot. Paris, 1822, 499-508.
- [15] Cattaneo, C., and Sulla conduzione Del Calore., *Atti Del Seminario Matematico e Fisico dell' Universita di Modena*, 3, 1948, 83-101.
- [16] Christov, C. I., On frame indifferent formulation of the Maxwell-Cattaneo model of finite-speed heat conduction, *Mechanics Research Communications*, 36, 2009, 481-486.
- [17] Nagendramma, V., Raju, C.S.K., Mallikarjuna, B., Shehzad, S.A., and Leelaratnam, A., 3D Casson nanofluid flow over slandering surface in a suspension of gyrotactic microorganism with Cattaneo-Christov heat flux, *Applied Mathematics and Mechanics*, 39(5), 2018, 623-638.
- [18] Makinde, O.D., Nagendramma, V., Raju, C.S.K., and Leelaratnam, A., Effect of Cattaneo-Christov heat flux on Casson nanofluid flow past a stretching cylinder, *Defect and Diffusion Forum*, 378, 2017, 28-38.
- [19] Malik, M.Y., Khan, M., Salahuddin, T., and Khan, I., Variable viscosity and MHD flow in Casson fluid with Cattaneo-Christov heat flux model: using Keller box method, *Int. J. Eng. Sci. Tech.*, 19(4), 2016, 1985-92.
- [20] Asif, M., Waseem, J., and Asim, A., Entropy and heat transfer analysis using Cattaneo-Christov heat flux model for a boundary layer flow of Casson nanofluid, *Results in Physics*, 10, 2018, 640-649.
- [21] Ibrahim, W., and Makinde, O.D., Magneto hydrodynamic stagnation point flow and heat transfer of Casson nanofluid past a stretching sheet with slip and convective boundary condition, *Journal of Aerospace Engineering*, 29(2), 2016, 04015037.
- [22] Kamran, A., Hussain, S., Sagheer, M., and Akmal, N., A numerical study of magneto hydro-dynamics flow in Casson nanofluid combined with Joule heating and slip boundary conditions, *Results in Physics*, 7, 2017, 3037-3048.
- [23] Nadeem, S., Rizwan, U.H., Akbar, N., and Khan, Z.H., MHD three dimensional Casson fluid flow past a porous linearly stretching sheet, *Alexandria Eng. J.*, 52(4), 2013, 577-582.
- [24] Hussain, T., Shehzad, S.A., Alsaedi, A., Hayat, T., and Ramzan, M., Flow of Casson nanofluid with viscous dissipation and convective conditions: A mathematical model, *J. Central South University*, 22, 2015, 1132-1140.
- [25] Sulochana, C., Ashwin Kumar, G.P., and Sandeep, N., Similarity solutions of 3D Casson nanofluid flow over a stretching sheet with convective boundary conditions, *J. Nigerian Math Soc.*, 35(1), 2016, 28-141.
- [26] Abolbashari, M.H., Freidoonimehr, N., Nazari, F., and Rashidi, M.M., Analytical modeling of entropy generation for Casson nano-fluid flow induced by a stretching surface, *Adv. Powder Tech.*, 26(2), 2015, 542-552.
- [27] Wasim, J., and Asim, A., Cattaneo-Christov based study of TiO₂-CuO/EG Casson hybrid nanofluid flow over a stretching surface with entropy generation, *Applied Nanoscience*, 8(4), 2018, 685-698.
- [28] Qing, J., Bhatti, M.M., Abbas, M.A., Rashidi, M.M., and Ali, M.E.S., Entropy Generation on MHD Casson Nanofluid Flow over a Porous Stretching/Shrinking Surface, *Entropy*, 18, 2016, 123.
- [29] Li, Z., Shahrajabian, H., Bagherzadeh, S.A., Hamid J., Arash K., and Tlili, I., Effects of nano-clay content, foaming temperature and foaming time on density and cell size of PVC matrix foam by presented Least Absolute Shrinkage and Selection Operator statistical regression via suitable experiments as a function of MMT content, *Physica A: Statistical Mechanics and its Applications*, 537, 2020, 122637.
- [30] Ullah, I., Khan, I., and Shafie, S., MHD natural convection flow of Casson nanofluid over nonlinearly stretching sheet through porous medium with chemical reaction and thermal radiation, *Nanoscale Research Letters*, 11, 2016, 527.
- [31] Afify, A.A., The influence of slip boundary conditions on Casson nanofluid flow over a stretching sheet in the presence of viscous dissipation and chemical reaction, *Mathematical Problems in Engineering*, 2017, 3804751, 1-12.
- [32] Ghadikolaei, S.S., Hosseinzadeh, K., Ganji, D.D., and Jafari, B., Nonlinear thermal radiation effect on magneto Casson nanofluid flow with Joule heating effect over an inclined porous stretching sheet, *Case Studies in Thermal Eng.*, 12, 2018, 176-187.
- [33] Thumma, T., Mishra, S.R., and Shamshuddin, M.D., Effect of heat generation and viscous dissipation on MHD 3D Casson nanofluid flow past an impermeable stretching sheet. In: Srinivasacharya D., Reddy K. (eds.) *Numerical Heat Transfer and Fluid Flow, Lecture Notes in Mechanical Engineering*, Springer, Singapore, 2019, 575-585.
- [34] Adomian, G., A review of the decomposition method in applied mathematics, *J. Anal. Appl.*, 135, 1988, 501-544.
- [35] Adomian, G., *Solving frontier problems of physics: The decomposition method*, Springer, Netherlands 1st Ed., 1994.
- [36] Hossein, J., and Varsha, D., Revised Adomian decomposition method for solving a system of nonlinear equations, *Applied Mathematics and Computation*, 175, 2006, 1-7.
- [37] Khan, U., Ahmed, N., Khan, S.I., Bano, S., and Mohyud-din, S.T., Unsteady squeezing flow of a Casson fluid between parallel plates, *World J. Modelling and Simulations* 10(4), 2014, 308-319.
- [38] Srinivas, J., Adesanya, S.O., Falade, J.A., and Nagaraju, G., Entropy generation analysis for a radiative micropolar fluid flow through a vertical channel saturated with non-Darcian porous medium, *Int. J. Appl. Comput. Math.* 3(4), 2017, 3759-3782.
- [39] Ebaid, A., Aljoufi, M.D., and Wazwaz, A.M., An advanced study on the solution of nanofluid flow problems via Adomian's method, *Applied Mathematics Letters*, 46, 2015, 117-122.
- [40] Manzoor, N., Maqbool, K., Bég, O.A., Shaheen, S., Adomian decomposition solution for propulsion of dissipative magnetic Jeffrey biofluid in a ciliated channel containing a porous medium with forced convection heat transfer, *Heat Transfer- Asian Research*, 48(2), 2019, 556-581.
- [41] Opanuga, A.A., Gbadeyan, J.A., and Iyase, S.A., Second law analysis of hydromagnetic couple stress fluid embedded in a non-Darcian porous medium, *IAENG International Journal of Applied Mathematics*, 47(3), 2017, 287-294.
- [42] Opanuga, A.A., Okagbue, H.I., Agboola, O.O., and Bishop, S.A., Second law analysis of Ion slip effect on MHD couple stress fluid, *Int. J. Mechanics*, 12, 2018, 96-101.
- [43] Thirupathi, T., Bég, O.A., and Kadir, Numerical study of heat source/sink effects on dissipative magnetic nanofluid flow from a non-linear inclined stretching/shrinking sheet, *J. of Molecular Liquids*, 232, 2017, 159-173.



- [44] Thirupathi, T., Chamkha, A.J., and Sheri, S.R., MHD Natural Convective Flow of Nanofluids past Stationary and Moving Inclined Porous Plate considering Temperature and Concentration gradients with Suction, *Int. J. of Numerical Methods for Heat and Fluid Flow*, 27(8), 2017, 1765-1794.
- [45] Sheri, S.R., and Thirupathi, T., Numerical study of heat transfer enhancement in MHD free convection flow over vertical plate utilizing nanofluids, *Ain Shams Engineering Journal*, 9, 2018, 1169-1180.
- [46] Thirupathi, T., and Mishra, S.R., Effect of viscous dissipation and joule heating on MHD Jeffery nanofluid flow with and without multi slip boundary conditions, *J. Nanofluids*, 7(3), 2018, 516–526.
- [47] Thirupathi, T., Bég, O.A., and Sheri, S.R., Finite element computation of magnetohydrodynamic nanofluid convection from an oscillating inclined plate with radiative flux, heat source and variable temperature effects, *Proc. IMechE Part N: J. Nanomaterials, Nanoengineering and Nanosystems*, 231(4), 2017, 179-194.
- [48] Aziz, A., Jamshed, W., and Aziz, T., Mathematical model for thermal and entropy analysis of thermal solar collectors by using Maxwell nanofluids with slip conditions, thermal radiation and variable thermal conductivity, *Open Physics*, 6, 2018, 123-136.
- [49] Thirupathi T., and Mishra, S.R., Effect of nonuniform heat source/sink, and viscous and Joule dissipation on 3D Eyring–Powell nanofluid flow over a stretching sheet, *J. of Computational Design and Eng.*, 2020, <https://doi.org/10.1093/jcde/qwaa034>
- [50] Wakif, A., Boulahia, Z., Ali, F., Eid, M.R., and Sehaqui, R., Numerical analysis of the unsteady natural convection MHD Couette nanofluid Flow in the presence of thermal radiation using single and two-phase nanofluid models for Cu–Water nanofluids, *Int. J. Appl. Comput. Math.*, 4, 2018, 81.
- [51] Wakif, A., Boulahia, Z., Mishra, S.R., Rashidi, M.M., and Sehaqui, R., Influence of a uniform transverse magnetic field on the Thermo - hydrodynamic stability in water-based nanofluids with metallic nanoparticles using the generalized Buongiorno's mathematical model, *European Physical Journal Plus*, 133, 2018, 181.
- [52] Dogonchi, A.S., Selimefendigil, F., and Ganji, D.D., Magneto-hydrodynamic natural convection of CuO-water nanofluid in complex shaped enclosure considering various nanoparticle shapes, *Int. J. Numer. Methods Heat Fluid Flow*, 29(5), 2019, 1663-1679.
- [53] Das, S., Chakraborty, S., Jana, R.N., and Makinde, O.D., Entropy analysis of unsteady magneto-nanofluid flow past accelerating stretching sheet with convective boundary conditions, *Adv. Appl. Math. Mech.*, 36(2), 2015, 1610.
- [54] Asai, S., *Magnetohydrodynamics in Materials Processing, Electromagnetic Processing of Materials*, Springer, Germany, 2011, 49-86.
- [55] Bég, O.A., Abdul Gaffar, S., Ramachandra Prasad, V., and Uddin, M.J., Computational solutions for non-isothermal, nonlinear magneto convection in porous media with Hall/ Ion slip currents and Ohmic dissipation, *Engineering Science and Technology - An International Journal*, 19, 2016, 377-394.
- [56] Thirupathi, T., and Magagula, V.M., Transient electromagnetohydrodynamic radiative squeezing flow between two parallel Riga plates using a spectral local linearization approach, *Heat Transfer-Asian Res.*, 49(1), 2019, 67-85.
- [57] Wakif, A., Chamkha, A.J., Thirupathi, T., Animasaun, I. L., and Rachid S., Thermal radiation and surface roughness effects on the thermo-magneto-hydrodynamic stability of alumina-copper oxide hybrid nanofluids utilizing the generalized Buongiorno's nanofluid model, *Journal of Thermal Analysis Calorimetry*, 2020, <https://doi.org/10.1007/s10973-020-09488-z>

ORCID iD

Thirupathi Thumma  <https://orcid.org/0000-0002-7993-5647>

S.R. Mishra  <https://orcid.org/0000-0002-3018-394X>

O. Anwar Bég  <https://orcid.org/0000-0001-5925-6711>



© 2021 by the authors. Licensee SCU, Ahvaz, Iran. This article is an open access article distributed under the terms and conditions of the Creative Commons Attribution-Non Commercial 4.0 International (CC BY-NC 4.0 license) (<http://creativecommons.org/licenses/by-nc/4.0/>).

How to cite this article: Thumma T., Mishra S.R., Anwar Bég O. ADM Solution for Cu/CuO –Water Viscoplastic Nanofluid Transient Slip Flow from a Porous Stretching Sheet with Entropy Generation, Convective Wall Temperature and Radiative Effects, *J. Appl. Comput. Mech.*, xx(x), 2021, 1–15. <https://doi.org/10.22055/JACM.2020.33137.2167>

